Aerospace Science and Technology, Volume 104, September 2020, Article number 105914
DOI: 10.1016/j.ast.2020.105914

Interplay of Unsteady Aerodynamics and Flight Dynamics of Transport Aircraft in Icing Conditions

D.I. Ignatyev[1], A.N. Khrabrov[2], A.I. Kortukova[3], D.A. Alieva[2], M. E. Sidoryuk[2], and S.G. Bazhenov[2]

[1] *Cranfield University, College Road, Cranfield, MK43 0AL, UK*

[2] *Central Aerohydrodynamic Institute (TsAGI), 1 Zhukovsky Str., Zhukovsky, Moscow Region, Russia, 140180*

[3] *Moscow Institute of Physics and Technology, 16 Gagarina Str., Zhukovsky, Moscow Region, Russia, 140180*

Abstract

Airframe icing causes significant degradation of aerodynamic characteristics and influences the flight safety. Wind tunnel study of longitudinal steady and unsteady aerodynamic characteristics of a transport aircraft in icing conditions is carried out in order to develop mathematical model of aerodynamics in the extended flight envelope. The wind tunnel results are validated through flight tests conducted for the real aircraft. Large, glaze-horn ice shapes, corresponding to holding flight phase, are considered. Influence of an ice protection system as well as its failure is examined. Effect of icing on the unsteady aerodynamics characteristics is studied not only through wind tunnel tests but also via analysis of subsequent influence on the flight dynamics of the aircraft. The conducted study shows that the ice shapes of the holding phase leads to reduced stall angle of attack (AoA), maximum lift, and longitudinal damping. Flight dynamics analysis demonstrates that dangerous aircraft behaviour in the form of high AoA departure and limit cycle oscillations (LCO) can be observed at smaller elevator deflections for the iced aircraft. Taking into account icing influence on the unsteady aerodynamics in the flight dynamics simulations revealed degradation of the dynamic response and deterioration of phase portraits of the system. Even for small AoA and elevator deflection the aircraft might be trapped into the basin of attraction of high-AoA LCO. In addition, incorporating icing effects in unsteady aerodynamics manifest larger amplitude of LCO.

Key words: Unsteady aerodynamics, flight dynamics, airframe icing, limit cycle oscillations, high incidence departure, wind tunnel test.

---

1. Introduction

Enabling flight safety in the presence of adverse conditions, such as those caused by environmental factors, is a challenging problem. Analysis of accident and incidence reports revealed that the significant part of the weather-related accidents were due to aircraft icing. Modern rules of the aviation authorities (for example, [1]) require guaranteeing flight safety of transport aircraft in icing conditions. Airframe icing is still an up-to-date problem, despite the fact that it has existed since the beginning of the aviation era. Over the past 90 years, techniques gradually increasing understanding of icing and improving fidelity of models of icing effects on performance, stability and control have been developed [2]. At the beginning, focus has been on wind tunnel studies of 2-dimensional subscale airfoils [3]–[6] and separate wings [2], [4], [7]. Further researches has been performed to investigate the integrated effects of icing on the aircraft performance, stability and control [2], [4], [7]–[10].

Many researchers were focused on the icing of the general aviation or business jet aircrafts because icing is generally more of a hazard to smaller aircraft [2], [8], [10]–[12]. Longitudinal dynamics of a general-purpose light airplane with twin turboprop engines was studied in [11]. A technique sensing the influence and location of ice on the same aircraft performance and control during trimmed flight was designed in [10]. Delta-model was used to simulate various icing effects of a business jet [12]. An analysis of the icing influence on the aerodynamics of transport aircrafts is payed attention in [7], [9], [13]. A very comprehensive review of the past studies on aircraft icing can be found in [14].

Most of the researches are aimed at studying the aerodynamics and flight dynamics of an iced aircraft at trim conditions that makes proper design of control algorithms. Nevertheless, modelling of flight dynamics in the extended flight envelope is crucial for understanding of reasons that might cause aircraft loss of control and, thus, helps to improve flight safety [15]–[17]. To support these activities, the technique for estimation of stability boundary of an aircraft in icing conditions based on the analyzing the region of attraction was proposed in [18].

The common approach for modelling icing effects on aerodynamics is restricted with a number of effects, such as increase of aerodynamic drag coefficient C_D, decrease of the maximum lift coefficient value C_L and the slope of lift coefficient curve $C_{L_\alpha} = \frac{dC_L}{d\alpha}$, decrease of the critical angle of attack (AoA) α, increase of the stall speed, changing of the pitching moment coefficient C_m. Dynamic wind tunnel tests of a sub-scale iced business jet showed that unsteady aerodynamic characteristics of the aircraft were affected by the ice accretion in the stall-region [19]. The current study is focused on the influence of icing effects on the unsteady aerodynamics of an aircraft of transport category and how these effects are transferred further into dynamic response of the system. Solid understanding of the interplay between aerodynamics and flight dynamics in icing conditions helps to improve the fidelity of simulations and, thus, increase flight safety, especially in case of presence of other adverse onboard or external conditions [20].

There are several types of ice accretion scenarios concerning different flight phases, namely, takeoff (including the ground roll, takeoff, and final takeoff segments), en route, holding, and approach/landing (including both the approach and landing segments). From the methodological point of view, the main purpose of this study is to improve fidelity of aerodynamic models in icing conditions and to bring understanding of necessity of increasing complexity in aerodynamic modelling via incorporating icing effects in the unsteady aerodynamic derivatives. To reach these goals, an experimental studying of the unsteady aerodynamic characteristic degradation caused by large, glaze-horn icing, corresponding to the holding flight phase was done. These ice shapes are taken into consideration since their relative dimensions are significantly large as compared to the other ice accretion types and the produced effect is very distinctive. As reported by different authors [2], [9], [19], influence of the large ice shapes on the aerodynamics can be evaluated using cost-effective small-scaled aircraft models with a reasonable precision.

The paper is organized as follows. Wind tunnel technique overview and the small-scaled model parameters are provided in Section 2. Description of the artificial ice shapes corresponding to ice accretion scenarios considered within this research is given in Section 3. In particular, large,

glaze horn ice shapes corresponding to holding phase is considered as a basic scenario. In addition, scenarios of operating Ice Protection System (IPS) during holding phase together with the IPS failure are examined. Results of wind tunnel tests are shown in Section 4. The wind tunnel results are compared with the results of flight tests carried out for a real aircraft [21] to validate the wind tunnel results obtained with a small Reynolds number model. Contributions to degradation of the aerodynamic characteristics caused by the ice accretion on the wing and on the tail are discussed. Section 5 overviews the mathematical models of icing effects used in the current study. Analysis of the icing on the flight dynamics is studied in Section 6. Finally, Section 7 concludes the paper.

2. Experiment overview

The main goal of the present section is to estimate the influence of aircraft icing on the longitudinal unsteady aerodynamic characteristics of the transport aircraft, which is a low-wing monoplane with a high aspect ratio wing, a conventional tail unit with a single vertical stabilizer and two wing-mounted engines. The wind tunnel model is the small-scale model of the aircraft. Reynolds number corresponding to the wind tunnel model is $\mathrm{Re} \approx 0.2 \cdot 10^6$. This parameter is calculated for the mean aerodynamic chord (Basic geometrical parameters of the model are provided in Table 1). The aircraft model inside the wind tunnel test section is shown in Fig.1. The model is mounted to a tail support strut

Table 1 Basic geometrical parameters of the wind tunnel model

Dimension	Value
Wing Reference area, S	0.12 m2
Wing Aspect ratio	9.8
Wing Span	1.11 m
Wing Mean aerodynamic chord, c_{mac}	0.123 m
Wing quarter-chord sweep	25 deg
Dihedral angle	7 deg
Horizontal tail relative reference area	0.26
Vertical tail relative reference area	0.2

Experimental studies of aerodynamic characteristics were conducted in low-speed wind tunnel T-103 of Central Aerohydrodynamic Institute (TsAGI) in two stages. At the first stage, the static characteristics were studied. The incidence angle α_0 was varied from -4 deg to 40 deg with 2 deg step. At the second stage, the dynamic derivatives were determined through a forced oscillation tests. During the forced-oscillation test the incidence was altered as follows [16]:

$$\alpha = \alpha_0 + A_\alpha \sin(2\pi ft + \vartheta_0) . \quad (1)$$

Oscillations were carried out with the amplitude $A_\alpha = 3°$, frequencies f = 0.5, 1.0, and 1.5 Hz for the mean angles of attack α_0 varying from -10 to 40°. While conducting the pitch forced oscillations the static derivatives $C_{L_\alpha}(\alpha), C_{m_\alpha}(\alpha)$, dynamic derivatives $C_{L_{\bar{q}}}(\alpha)+C_{L_{\dot{\bar{\alpha}}}}(\alpha)$ and $C_{m_{\bar{q}}}(\alpha)+C_{m_{\dot{\bar{\alpha}}}}(\alpha)$ were obtained together with the mean values of $C_{L_0}(\alpha)$ and $C_{m_0}(\alpha)$.

Fig.1. Fully iced aircraft model installed on the tail support strut in the wind tunnel test section.

Both types of the experiments were carried out for the clean aircraft model, namely, for the aircraft model without artificial ice shapes, and for the iced aircraft model. Different types of the aircraft icing were studied. All types of icing configurations are given in Section 3 The wind tunnel flow velocity was $V_0 = 25$ m/s. Five-component strain gauge balance located inside the model with the reference center at 0.25 c_{mac} was used to measure the aerodynamic loads.

The flight tests were also conducted for the real aircraft for the clean configuration and for the configuration with artificial large, glaze-horn ice shapes. The

aerodynamic coefficients were identified using the transition processes obtained in manoeuvres during the flight tests [21].

3. Artificial ice shapes

The present research is focused on studying the degradation of the aerodynamic characteristics caused by large, glaze-horn icing, corresponding to the holding phase. Contributions to the degradation of the aerodynamic characteristics caused by the ice accretion on the wing and on the tail are evaluated in the experiment. These scenarios are taken into considerations since the relative dimensions of these ice shapes are significantly large as compared to the other scenarios. As reported by different authors [2], [7] influence of the large, glaze-horn ice shapes on the aerodynamics can be evaluated using small-scaled aircraft models. The other ice accretion scenarios are also have a great impact on the flight safety but require much more expensive experiments using large-scale models since the Reynolds number significantly influences on the results for such types of experimental simulations [2]. In addition, a correct simulation of ice shapes, including roughness, can be very crucial while studying the stages with relatively small ice shapes (ground roll, takeoff, final takeoff segments, and etc.) This makes it very complicated to produce and install properly the ice shapes on the relatively small wind tunnel models.

Artificial ice shapes were placed on the wing, vertical and the horizontal tail (HT). The location scheme of ice shapes is shown in Fig.2.

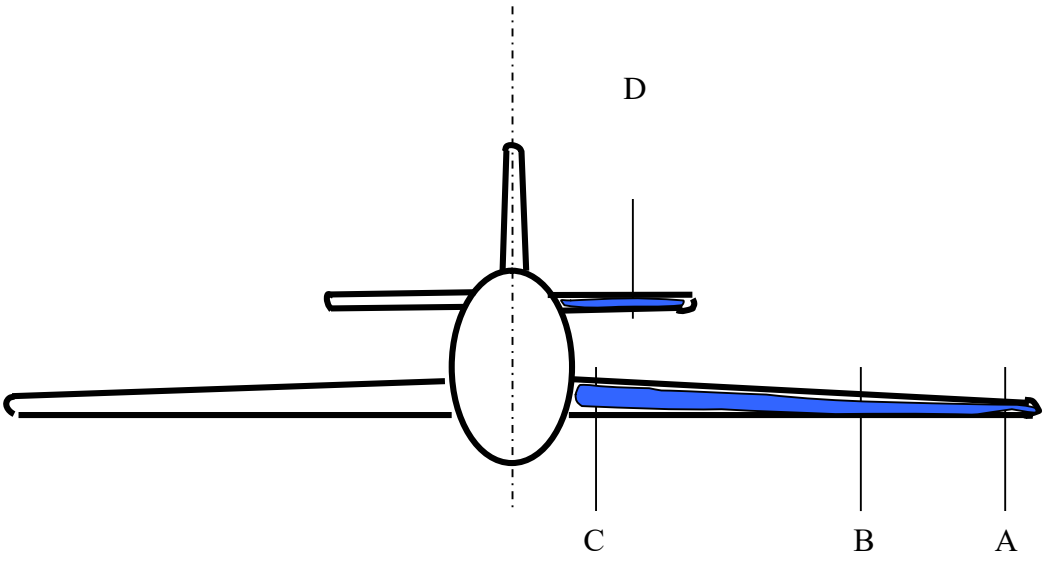

Fig.2. Scheme of location of ice shapes.

Influence of the icing effects on the longitudinal aerodynamic characteristics were studied in the experiments when the artificial ice shapes were installed separately on the wing or on the HT. Ice shape forms were obtained using an engineering technique proposed in [22] and shown in Fig.3.

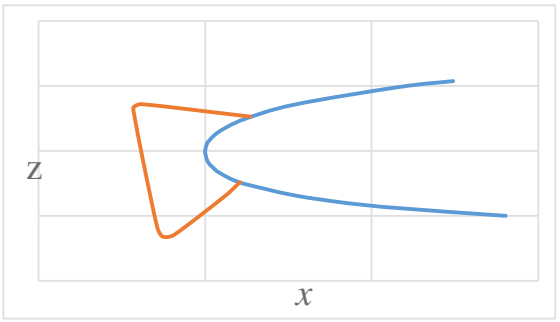

a) Section A : Holding phase

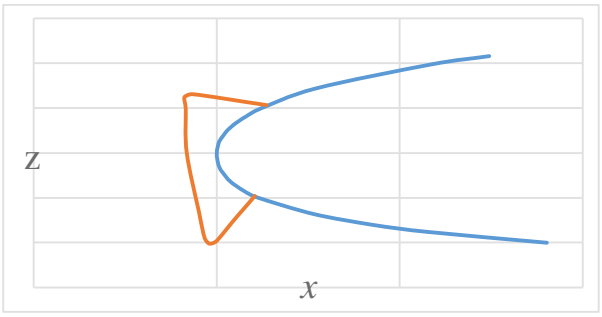

d) Section A: Failure of the ice protection system

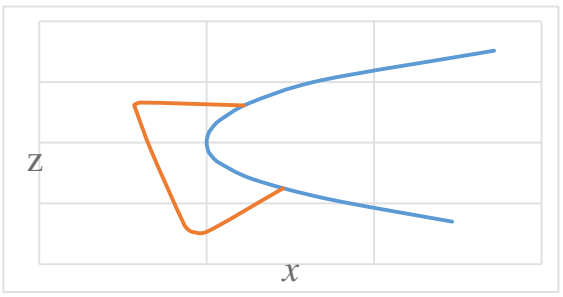

b) Section B: Holding phase

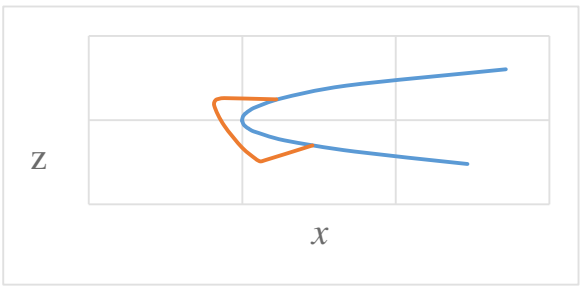

e) Section B: Failure of the ice protection system

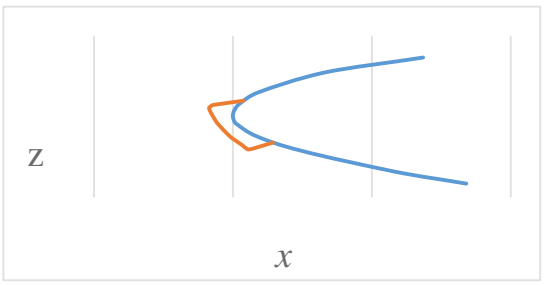

c) Section C : Holding phase

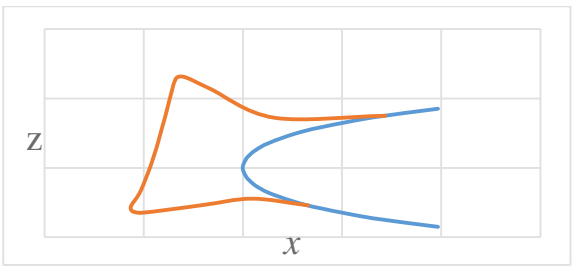

f) Section D: Icing of horisontal tail

Fig.3. Artificial ice shapes

Aircraft of the transport category are normally equipped with a wing IPS to prevent or, at least, reduce ice accretion on the wing. In the current study, it is considered that the aircraft has a heated leading edge system covering the most part of the wing, namely, between the engine pylon and the tip chord. Operation of the IPS leads to melting of the ice in the heated region. A possible IPS failure is put into consideration in this study. In the case of IPS failure, the leading edge ice

has smaller dimension, however, holds the same horn shape (see Fig.3). During the wind tunnel tests, to simulate the IPS operation, there were no ice shapes placed in the zones of heating.

The artificial ice shapes for right-hand side of the wing is symmetrical. The forms of the artificial ice shapes in sections A-D corresponding to the holding phase and in sections A and B corresponding to the failure of the ice protection system are given in Fig.3.

The artificial ice shapes were printed with the printing precision of 0.2 mm. The examples of the printed artificial ice shapes are shown in Fig.4a. Photo of the model with installed artificial ice shapes corresponding to the holding phase is shown in Fig.4b. One can see that the artificial ice shapes are mounted on the wing and the tail unit.

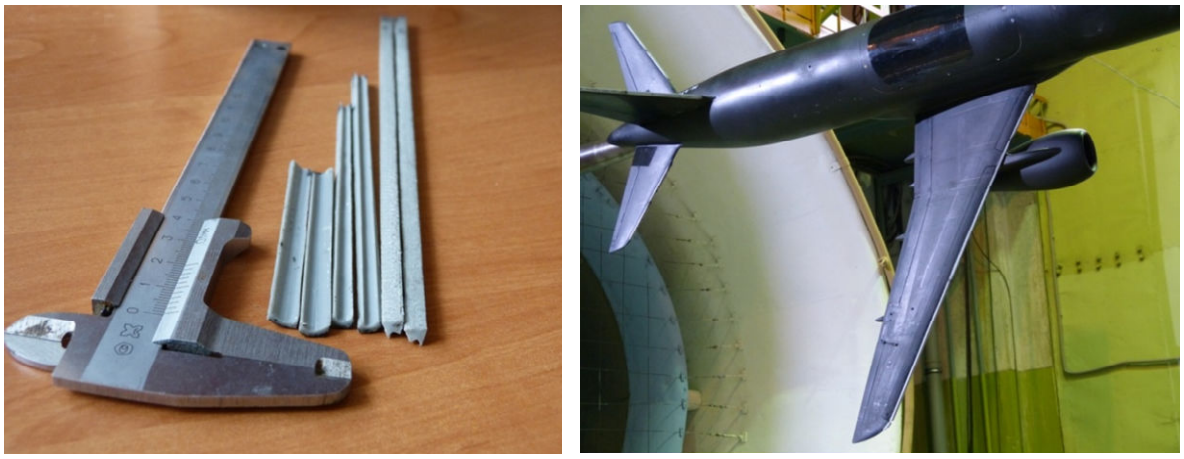

a b

Fig.4. Printed artificial ice shapes: a – examples, b – installed on the aircraft model

4. Experimental results

4.1. Static tests

The wind tunnel static test results obtained for the lifting force coefficient effected by the airframe icing are given in Fig.5. The flight test results are also provided for the analysis. From the comparison of the wind tunnel and flight test results one can conclude the following. The results obtained for the wind tunnel aircraft model (small Reynolds number) and the real aircraft differ in significant way for the clean configuration, however, the results obtained for the configurations with artificial ice shapes (AIS) are quite similar. This gives us opportunity to evaluate the main

tendencies of aerodynamic characteristics of the aircraft with the large, glaze horn ice using small scaled models in wind tunnel experiments.

To distinguish an influence of the wing and the HT icing on the aerodynamic characteristics the wind tunnel studies were carried out for the different icing configurations, namely, for the fully iced configuration (ice shapes on the wing and the HT), for the iced wing model (ice shapes on the wing only) and the iced HT model (ice shapes on the HT only). One can see that the curves of the aerodynamic characteristics in Fig.5 corresponding to the models with iced wing and the fully iced model are very similar.

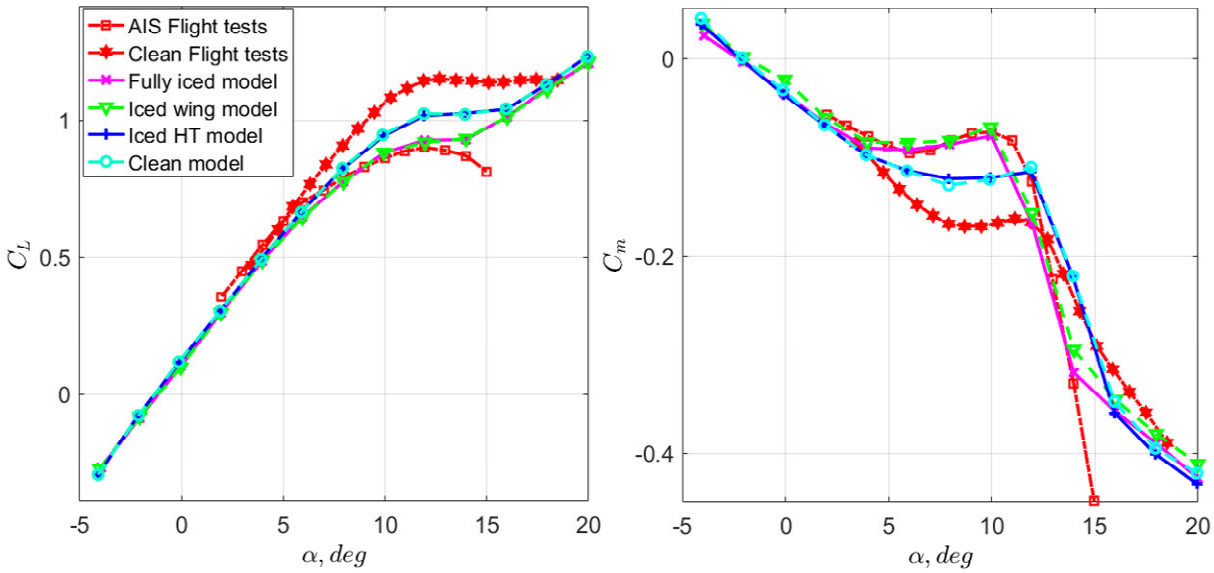

Fig.5. Longitudinal aerodynamic characteristics

This coplotting gives us the insight that the main contribution to degradation of the longitudinal aerodynamic characteristics, both for C_L and C_m, are caused by icing of the wing. Thus, the considered configurations can be divided into two groups, namely, the iced wing group that includes configuration with ice shapes at the wing and the fully-iced configuration and the clean wing group that includes configuration with ice shapes on the HT and the clean configuration. However, reduction in the lifting force because of icing is not very significant till AoA = 10 deg. Such behaviour is comparable with the results obtained for the Generic Transport Model (GTM) by Broeren et al. [9], which has a similar aircraft geometry. The flow-visualization images obtained in [9] revealed that incipience and evolution (at $\alpha > 4$ deg) of a spanwise-running vortex along the

leading-edge separation bubble above the upper surface of the wing was the dominant feature of the flow field. This vortex was observed in the leading-edge separation bubble in both the clean and iced configurations. This flow field structure can be explained with a schematic representation proposed by Poll [23] and shown in Fig.6.

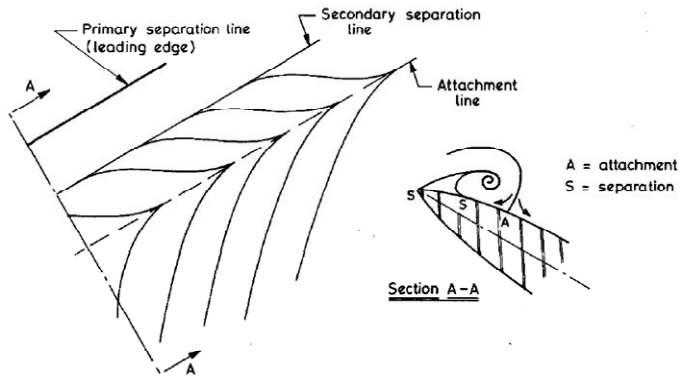

Fig.6. Flow field structure above the wing from [23]

According to analysis performed by Broeren et al. [9], prior to stall, the vortex core was close to the wing surface and laid approximately parallel to the leading edge. For AoA near stall, two flow structures were observed: one between the engine and fuselage and one outboard of the engine (Fig.7 a). In the latter structure, the spanwise vortex angled downstream and off the surface resulting in separated and reverse flow on the outboard portion of the wing (Fig.7 b). Similar structure was for the clean and iced configurations and explain the small degradation of the lift force of the iced configuration at small angles of attack as compared to the clean one. However, it should be noted that the aerodynamic characteristics of the clean configuration is significantly determined by the Reynolds number as it is shown in Fig.5, and therefore, we cannot rely on the results obtained for the clean wing. Meanwhile, results obtained for the iced configuration looks reasonable.

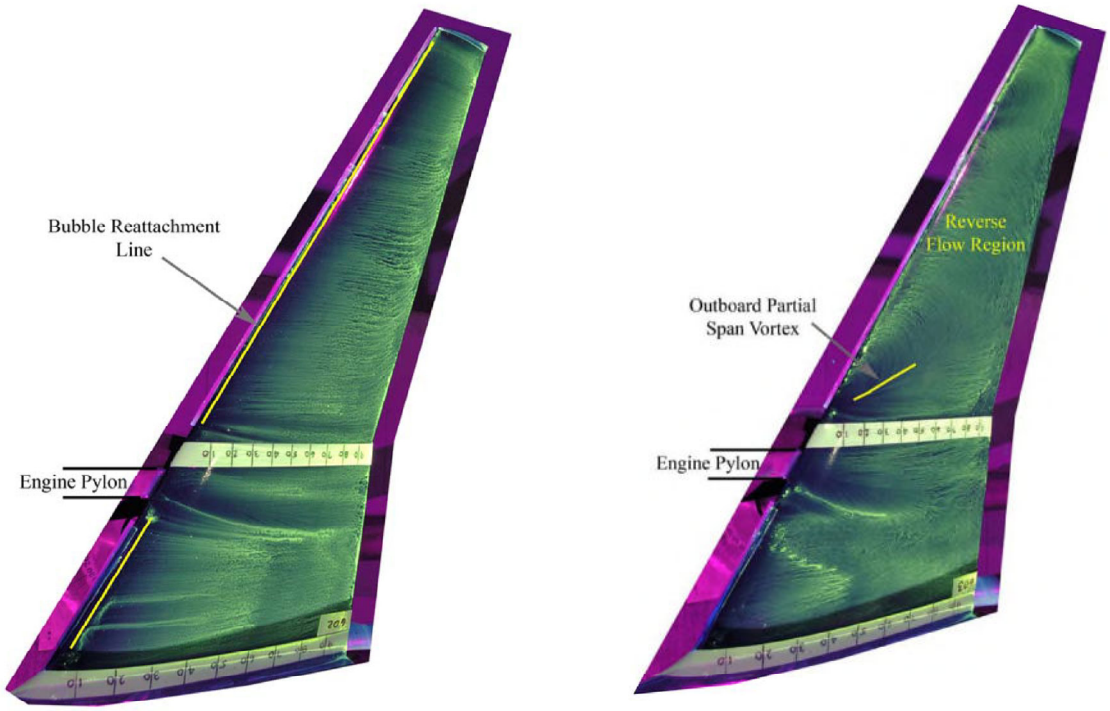

a b

Fig.7. Surface-oil flow visualization on the right wing with artificial ice shape β = 0 deg, a) α = 8 deg, b) α = 12 deg (from [9]).

One of the tangible effects of the wing icing that can be observed from the analysis of Fig.5 is a reduced stall AoA, namely, it is two degrees lower. According to the flow-visualization analysis provided in [9], ice forms causes earlier flow topology reconfiguration.

Unlike the lifting force, the icing effect on the pitching moment characteristics is more significant (see Fig.5). The wing ice reduces stability of the aircraft, increasing pitching moment. The other effect of the wing icing is that the aircraft has higher level of static instability C_{m_α} in the pre-stall region. In the region $4 < \alpha < 10$ (for the iced configuration), the pitching moment characteristics changes slope inclination, making the aircraft statically unstable. Possible explanation of this phenomenon is given in [9], where the authors showed that the spanwise-running vortex along the leading-edge separation bubble is formed in this AoA region. With further AoA increase, the vortex break down with formation of a massive separation region above the upper surface, causing the stall at $\alpha = 10$ deg, is observed. Influence of the pitching moment characteristics alteration due to icing on the flight dynamics will be discussed in Section 6.

Influence of the IPS on the lifting force and pitching moment coefficients was also studied. The results are provided in Fig.8.

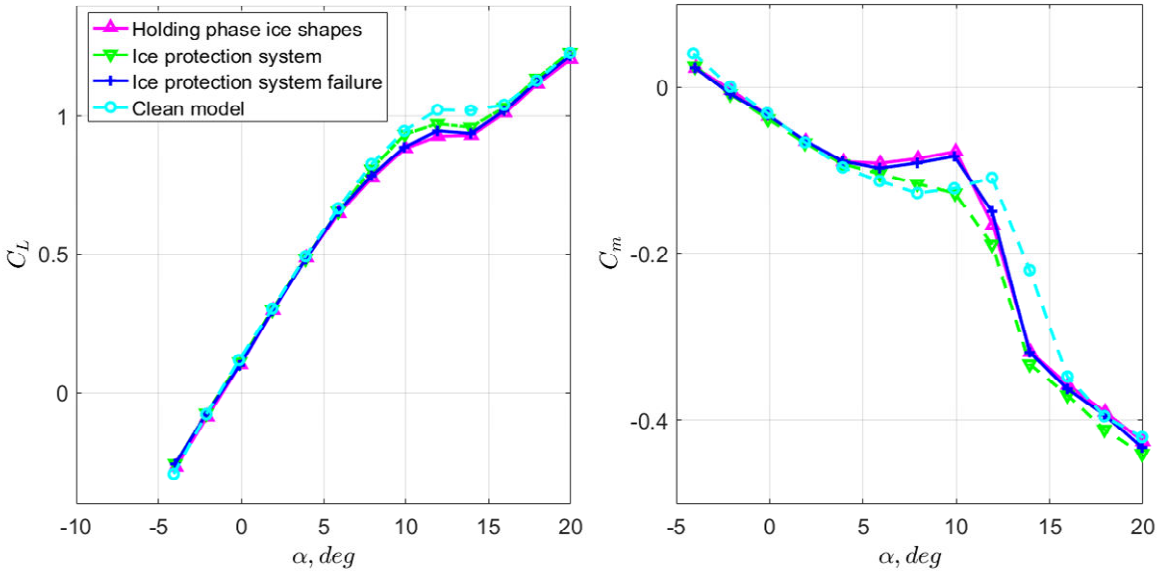

Fig.8. Ice protection system influence

IPS causes melting of the ice in the heating zones located on the leading edge, and, thus, improves aerodynamic performance of the aircraft. In particular, less reduction of the C_L and value of static instability $C_{m_\alpha} > 0$ at $6 < \alpha < 10$ is observed. In the case of IPS failure, quite large ice shapes, which are demonstrated in Fig.3, accrete on the leading edge of the wing. From Fig.8 one can see that behaviour of aerodynamic characteristics in the case of IPS failure is very similar to the fully iced model.

4.2. Dynamic tests

The small amplitude forced oscillations are dedicated to determine the unsteady aerodynamic derivatives. The results for the derivatives of the lift coefficient and pitching moment coefficient are given in Fig.9.

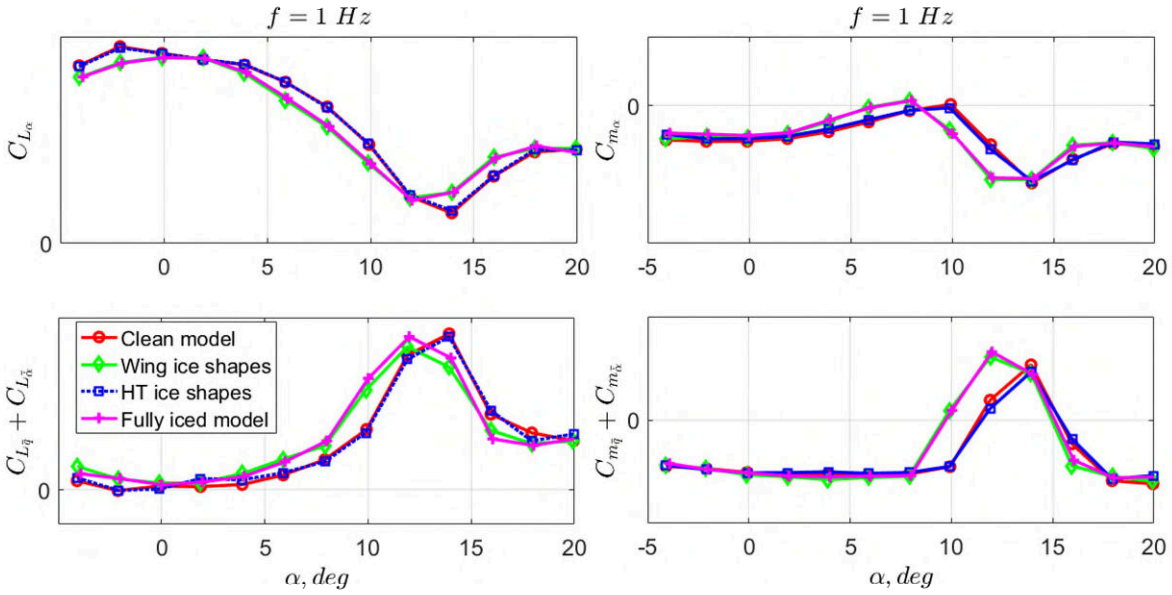

Fig.9. Unsteady aerodynamic characteristics $f = 1$ Hz.

One can determine that the aerodynamic derivatives obtained for the clean configuration are similar to results for the configuration with HT-ice, and results obtained for the iced wing are similar to those obtained for the fully iced configuration. This output correlates with the static test results, which state that degradation of the aerodynamic characteristics are mostly determined by the wing icing.

Regardless of the fact that the ice shapes have a minor effect on the static lilt force coefficient (Fig.5), we can notice an alteration of the dynamic characteristics behaviour at $\alpha > 6$ deg. As it was mention before, in the region $4 < \alpha < 8$ the spanwise-running vortex is formed, and presence of large glaze-horn type shapes effects on the flow pattern. The extreme points of static $C_{L_\alpha}(\alpha), C_{m_\alpha}(\alpha)$ and dynamic derivatives $C_{L_{\bar{q}}}(\alpha) + C_{L_{\dot{\bar{\alpha}}}}(\alpha)$ and $C_{m_{\bar{q}}}(\alpha) + C_{m_{\dot{\bar{\alpha}}}}(\alpha)$ for the iced wing configurations move to lower angles of attack ($\alpha = 12$ deg) as compared to the clean wing configuration ($\alpha = 14$ deg). One can see that presence of wing icing causes degradation of the aerodynamic characteristics at smaller angles of attack (8 deg instead of 10 deg). Thus, the region of nonlinear variation of aerodynamic derivatives is extended to lower angles of attack due to presence of ice shapes on the wing. Particularly, the pitch damping characteristics has a positive value in the wider region $10 \le \alpha \le 15$ for iced wing configurations as compared to $12 \le \alpha \le 15$ for the clean wing configurations. This fact negatively influences the flight safety since it increases a

possibility of the aircraft to be trapped into the basin of attraction of a high-AoA trim point. The intensity of the positive damping increases for the iced wing configurations.

Influence of the oscillation frequency on the unsteady aerodynamic characteristics is demonstrated with pitch moment derivatives in Fig.10, lifting force derivatives exhibit the same tendencies. Fully iced and clean configurations were considered.

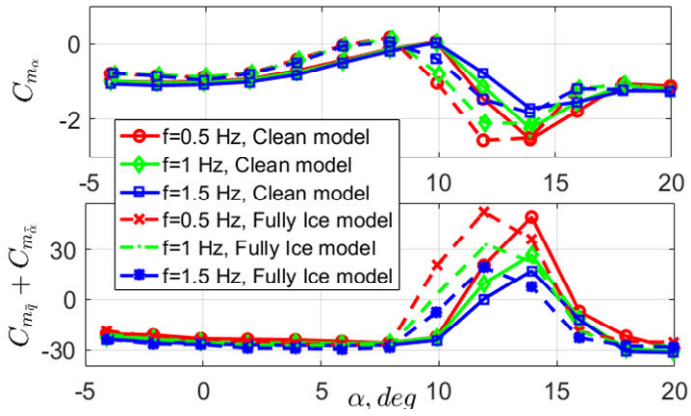

Fig.10. Influence of oscillation frequency on pitching moment derivatives

The results demonstrate the dependence of pitch moment derivatives on the oscillation frequency for both clean and iced aircraft. The main difference is that for the iced model the region of positive damping is extended to the smaller angles of attack.

Influence of the IPS on the unsteady lift force coefficients is very limited (Fig.11). However, the IPS has effect on the pitch moment coefficient, namely, it improves the static stability derivative C_{m_α} and increases pitch damping $C_{m_{\bar{q}}}(\alpha)+C_{m_{\dot{\bar{\alpha}}}}(\alpha)$ in the post-stall region. In the conditions of the system failure, the aerodynamic derivatives are very similar to the fully iced aircraft characteristics.

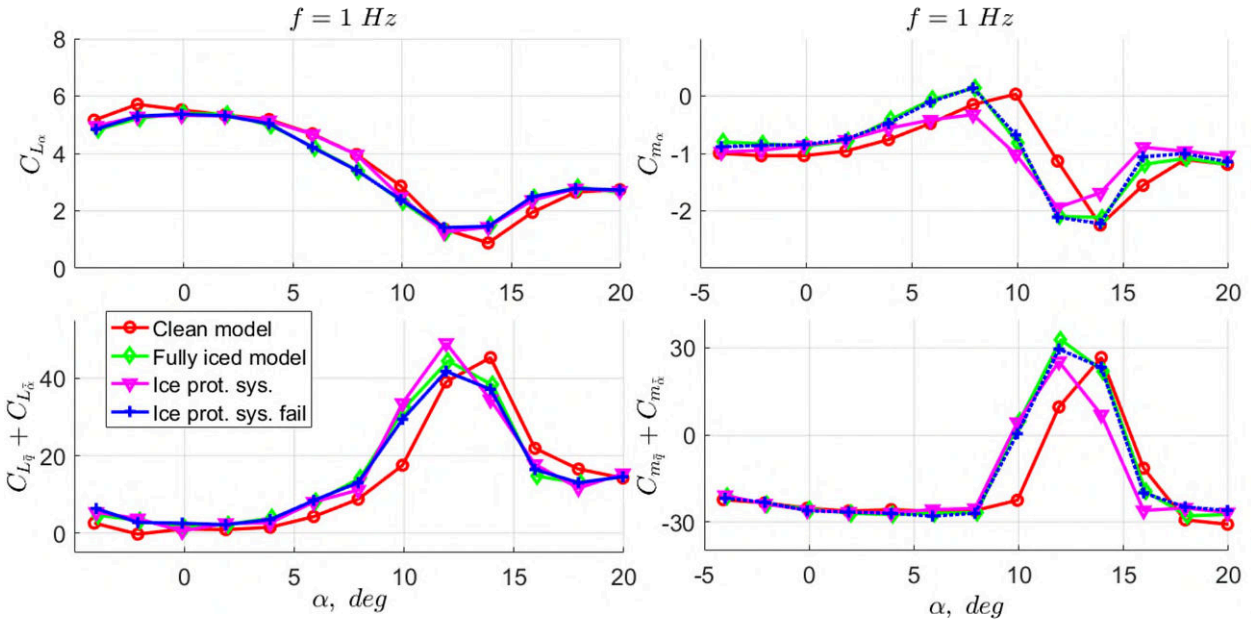

Fig.11. Lift force and pitch moment dynamics derivatives: influence of the ice protection system

5. Mathematical model

Experimental results revealed strongly nonlinear behaviour of the aerodynamic characteristics in the pre-stall and stall region, which is caused by the development of spanwise-running vortex. In the forced oscillation tests, regions of instabilities, where the static and the dynamic derivatives change sign, are revealed. Stability of the aircraft in the pre-stall region is highly influenced by interaction between the dynamics of the flow structure reconfiguration and aircraft flight dynamics itself. Several approaches were used to develop mathematical models of aerodynamics and flight dynamics in the similar conditions [16], [24]–[30]. In [30] simple approach based on spline approximation were proposed to describe nonlinear unsteady aerodynamic characteristics.

The model of longitudinal unsteady aerodynamic characteristics is developed using the approach proposed in [30], where it was demonstrated that aerodynamic characteristics of transport aircraft could be represented in the following form

$$C_i(\alpha,\bar{q}) = C_{i_{st}}(\alpha) + C_{i_{unst}}(\alpha,\bar{q}) + C_{i_\delta}\delta\,, \qquad (2)$$

here $C_i = \{C_L, C_D, C_m\}$ are lift, drug and pitch moment coefficients. Such approach was proven to be powerful enough to simulate the nonlinear behaviour of aerodynamic characteristics in the

extended flight envelope, e.g. hysteresis and dependencies on prehistory of motion, while having a very simple form. Eq. (2) is intuitive representation of aerodynamic characteristics, where $C_{i_{st}}(\alpha)$ is a static term, $C_{i_{unst}}(\alpha,\bar{q})$ is a term, describing all unsteady effects and $C_{i_\delta}\delta$ is a control contribution term. Using this form we can distinguish influence of icing on steady and unsteady aerodynamics.

To investigate the influence of the icing on the steady and unsteady aerodynamics and understand how this could produce further effect on the nonlinear flight dynamics we developed three separate mathematical models of aerodynamics in the form of Eq. (2).

For model No. 1, the icing effects are taken into account only for the static terms $C_{i_{st}}(\alpha)$ in Eq. (2), while for model No.2 the icing effects are also introduced in unsteady aerodynamics terms $C_{i_{unst}}(\alpha,\bar{q})$. Normally, for engineering applications [2], [10], [12], [31], a corruption of steady aerodynamics due to airframe icing is only of interest since the main influence on the flight dynamics could be transferred through these parameters. Nevertheless, the current research is also focused on alteration of unsteady aerodynamics and flight dynamics due to icing. Both models are compared with the non-icing configuration. Therefore, model No. 3 is the model, in which the static and the dynamic components in representation (2) are not degraded due to the icing effects.

The experimental results of static and dynamic tests of small-amplitude oscillations were used for the model development. Splines are used to interpolate the experimental data obtained for $C_{i_{st}}(\alpha)$, $C_{i_\delta}\delta$ and $C_{i_{unst}}(\alpha,\bar{q})$.

6. Flight dynamics studies

6.1. Short-period motion

Understanding of nonlinear dynamics and prediction of a region of attraction generated by critical regimes with respect to degradation of unsteady aerodynamics due to icing is very important for stall prevention and also for a recovery strategy design.

To highlight the effect produced by the changings of unsteady aerodynamics due to icing we firstly compared performance of the aerodynamics models Nos. 1-3 via simulating the short-period motion dynamics model, considering that the velocity is fixed and the path is rectilinear [32]

$$\begin{aligned} \dot{\alpha} &= q, \\ \dot{q} &= \frac{\rho V^2 S \bar{c}}{2I} C_m. \end{aligned} \tag{3}$$

where ρ is the air density, V is velocity, S is a wing area, $\bar{c}$ is a mean aerodynamic chord, I is an inertia moment and the pitch moment coefficient is given in the form of Eq. (2).

Let us first compare the dynamics of the clean and the fully iced aircrafts. Trim curves obtained for the clean aircraft model (Model No. 3) and the model with icing effects both in steady and unsteady coefficients (Model No. 1) are shown in Fig.12 with blue and red lines correspondingly. These curves provides trimming angle of attack for different elevator deflections.

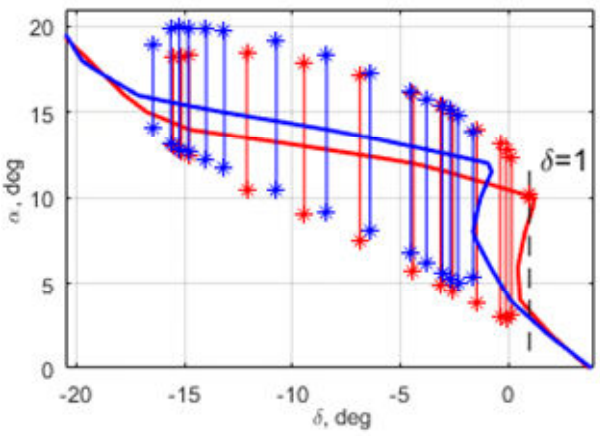

Fig.12. Trimming curves corresponding to iced (red) and clean (blue) configurations

One can see that curves obtained for the clean and the iced configurations coincide for small angles of attack ($0 \le \alpha \le 2$). Further deflection of the elevator with subsequent increase in angle of attack leads to deviation of the iced trim curve from the clean one. For a certain range of elevator deflections the steady state solution becomes a non-unique and three trim AoA could be achieved at the same elevator deflection. One trim solution corresponds to small incidence and third corresponds to high incidence. Further deflection of elevator causes loss of stability in the form of LCO, vertical lines represent the amplitude of these oscillations. High-AoA departure and LCO are observed for both models, however, these nonlinear phenomena observed at different control inputs. From the presented results, one can see that the loss of stability for the iced configuration is observed for smaller incidence and smaller angles of elevator

deflections, namely, AoA is equal to 12 degrees for the configuration without ice, and 10 degrees for the iced configuration.

Trim curves obtained for the model with icing effects in steady aerodynamic characteristics (Model No.1) and for the model with icing effects introduced both in the steady and unsteady parts (Model No. 2) are presented in Fig.13. Amplitudes of LCO are shown with vertical lines with stars in the same figure.

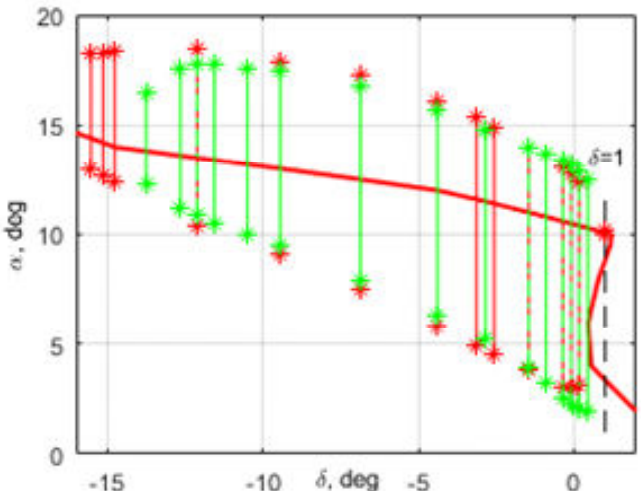

Fig.13. Trimming curves of Models 1 (icing effects in steady aerodynamic characteristics - green) and 2 (icing effects in steady and unsteady aerodynamic characteristics - red) for the short-period motion.

Both models have the same trim curve, because the trim solution is determined by the static characteristics. Nevertheless, if icing effects are considered for the unsteady part of (2), the bifurcation in the form of LCO arises at smaller deflection of the elevator and at smaller angle of attack.

The qualitative analysis of nonlinear dynamics in the phase plane of the state variables (q and α) for the elevator deflection $\delta = 1$ deg is given in Fig.14. For both models there are three equilibrium points $\alpha_1 \approx 3.4$ deg, $\alpha_2 \approx 8.7$ deg, and $\alpha_3 \approx 10$ deg, which are determined by the static pitch moment characteristics. However, behaviours of the models are different in these points. For Model No.1, which has the icing degradation only in the static characteristics, the first point is the stable foci, the second point is the saddle point and the third point is the unstable foci. For the current state variables, all trajectories finish at the small incidence equilibrium point $\alpha_1 \approx 3.4$ deg, at which the stability of the aircraft is ensured. For Model No.2, which has the icing influence not only in the static characteristics but also in unsteady characteristics, the first equilibrium point is still the stable foci at small angles of attack ($\alpha_1 \approx 3.4$

deg) and the second one ($\alpha_2 \approx 8.7$ deg) is still the saddle point. The third point ($\alpha_3 \approx 10$ deg) being the unstable foci has now a small amplitude orbitally stable limit cycle around this point.

This limit cycle has a basin of attraction. Some trajectories from this basin are shown with a red colour on the left subplot of Fig.14. From the safety point of view, this phase portrait means that, even at small AoA, aircraft could be trapped to the attraction domain of high-AoA equilibrium point with possible consequence of the aircraft stall.

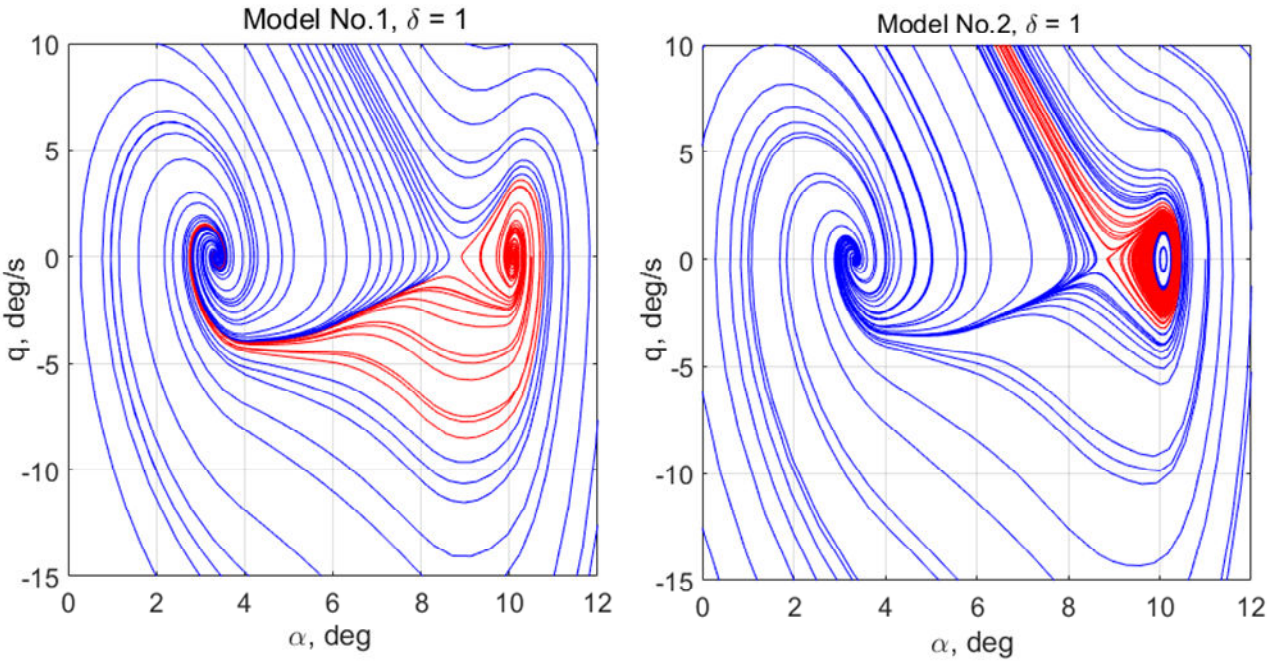

Fig.14. Phase portraits for Models Nos. 1 and 2.

6.2. Longitudinal motion

Further analysis is performed for the general case of longitudinal motion:

$$
\begin{aligned}
&\dot{\theta} = q, \\
&\dot{\alpha} = q + \frac{1}{mV}\left(mg\cos(\theta-\alpha) - \frac{C_L \rho V^2 S}{2}\cos\alpha - \left(T - \frac{C_D \rho V^2 S}{2} \right)\sin\alpha \right), \\
&\dot{q} = \frac{\rho V^2 S\, \bar{c}}{2I} C_m, \\
&\dot{V} = \frac{1}{m}\left(-\frac{C_L \rho V^2 S}{2}\sin\alpha + \left(T - \frac{C_D \rho V^2 S}{2} \right)\cos\alpha - mg\sin(\theta-\alpha) \right),
\end{aligned}
\tag{4}
$$

where the θ is a pitch angle, m is a mass, T is a trust. Here we are more focused on the stability of the aircraft, thus, we assumed that increase in drag coefficient $\Delta C_{D_{ICE}}$ due to icing is fully compensated by the additional thrust ΔT.

Trim curves obtained for the clean model and two models with icing effects in aerodynamic characteristics (Model No.1 and Model No. 2) are presented in Fig.15. LCO amplitudes are shown with vertical lines with stars in the same figure.

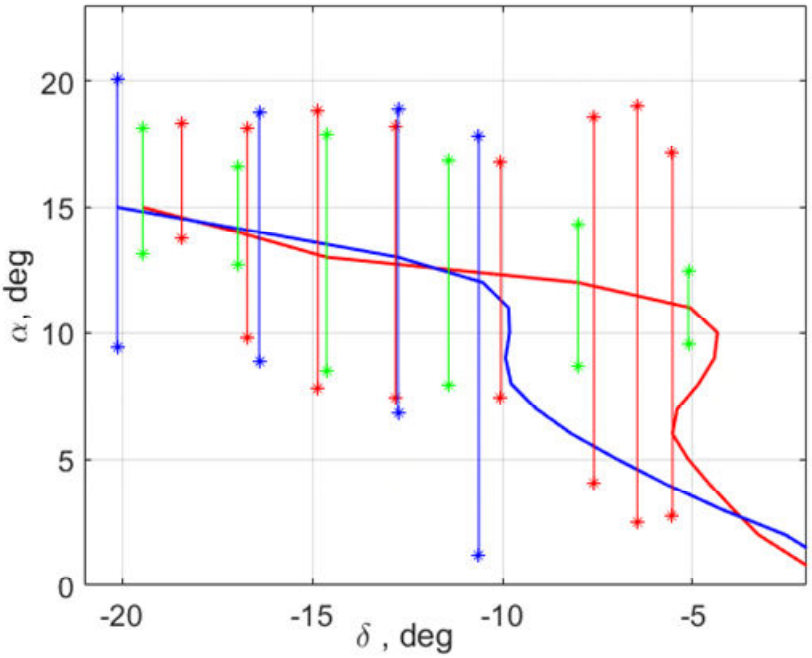

Fig.15. Trimming curves of the clean model (blue), the model with icing in steady characteristics (green) and the model with icing in steady and unsteady characteristics (red).

Similar to short-period case, the trimming curves for Models 1 and 2 coincide. For small incidence, both iced and clean configurations retain stability. With further increase of the elevator deflection, we can observe a saddle-point bifurcation at $\delta \approx -4.5$ deg. For the elevator deflection $-5.5 \le \delta \le -4.5$ deg, three solutions are possible for AoA. Greater increase of elevator causes another bifurcation and arise of LCO as a result. For the clean configuration, instability in the form of high-AoA departure and LCO is observed at greater values of elevator deflection and incidence.

Step responses of system (4) for Models 1-3 are provided in Fig.16. In the considered simulation scenarios, the aircraft is initially trimmed at $\alpha_0 = 4$ deg, and at t = 60 sec a step-wise control input $\Delta\delta = -1$ deg is demanded.

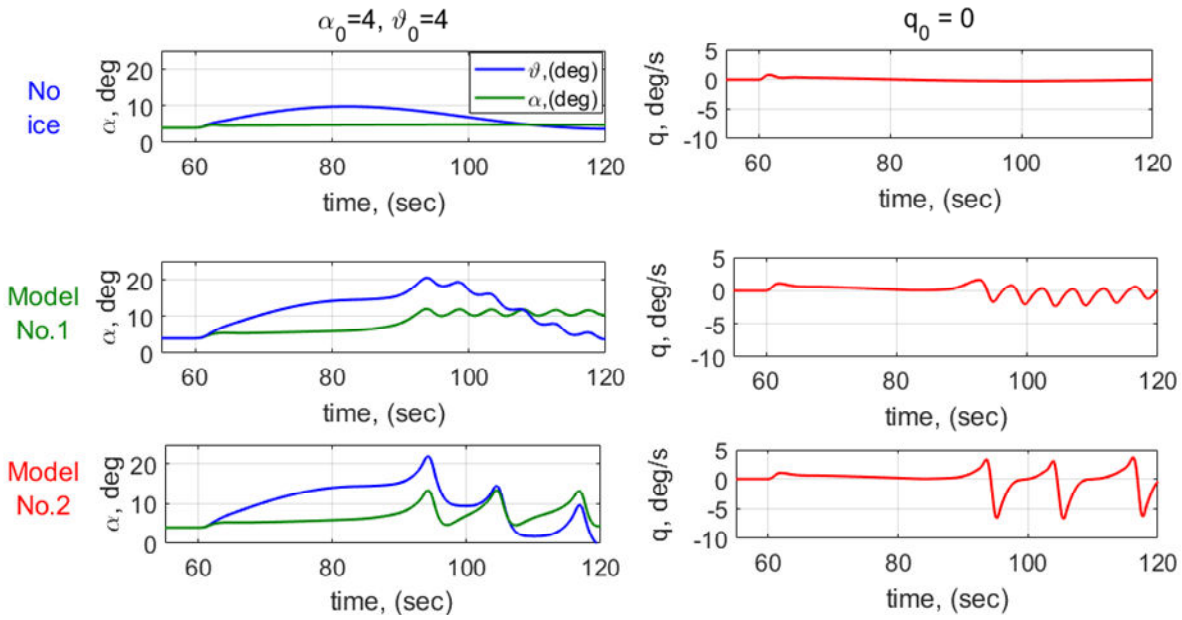

Fig.16. Step response at $\alpha_0 = 4$ deg to the control input $\Delta\delta = -1$ deg.

The clean aircraft remains stable in the considered case. Both mathematical models of iced aircraft aerodynamics exhibit dangerous instable behaviour with a high AoA departure and a LCO. However, instabilities observed in two models of icing effects on the aerodynamics are different. Oscillations in Model No.1 are almost harmonically of relatively small amplitude ($\Delta\alpha = 1$ deg) and around the equilibrium point $\alpha = 11$ deg. In Model No.2, the oscillation amplitude is larger, $\Delta\alpha = 10$ deg, however, oscillation frequency is lower as compared to Model No.1. LCO of Model No.2 represents trajectories between two equilibrium solutions and has a fast part of the trajectory (nose-down motion) and slow (nose-up motion) [33].

Step responses of system dynamics (4) for aerodynamics models 1-3 for trim angle $\alpha_0 = 6$ deg are provided in Fig.17.

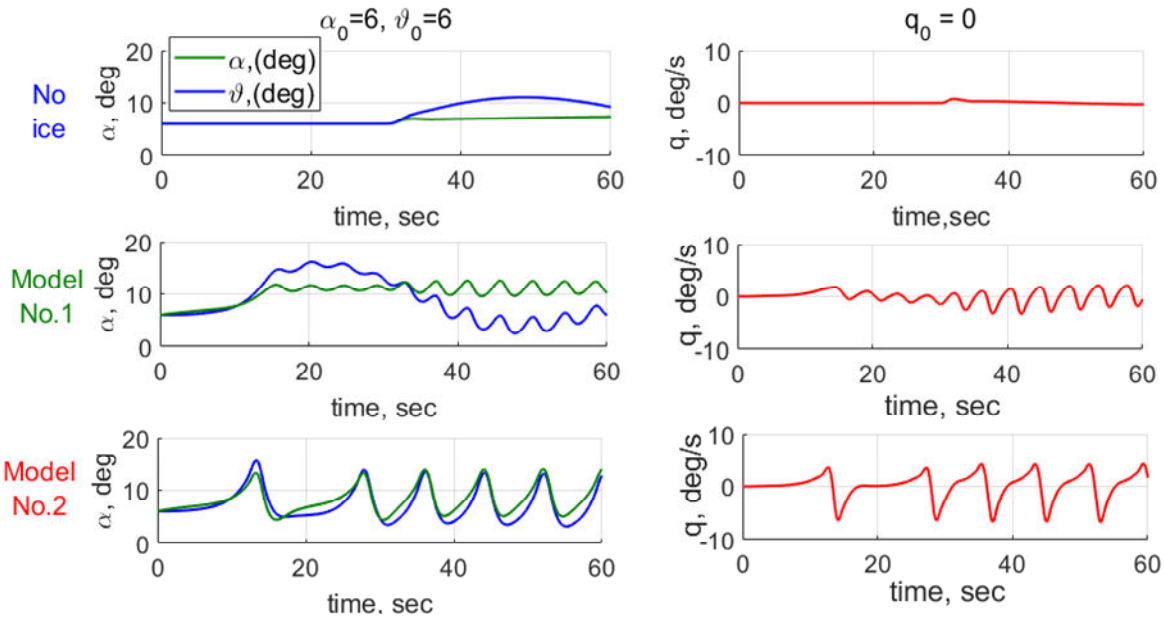

Fig.17. Step response at $\alpha_0 = 6$ deg to the control input $\Delta\delta = -1$ deg.

Similar to the previous example, the clean aircraft maintain the stability, keeping the small AoA with a highly damped transition process after applying the control input. According to Fig.15, $\alpha = 6$ deg is unstable equilibrium for both models with icing effects, so one can observe the oscillations in the system for Models No1 and 2 at this trim angle before demanding the control input. At *t*=30 sec, the control input $\Delta\delta = -1$ deg is demanded that results in alteration of the LCO for both models, the amplitude is increased for Model No.1, and the frequency is increased for Model No. 2.

7. Conclusion

Enabling flight safety in the presence of adverse conditions, such as those caused by environmental factors is a very important problem.

Complex analysis of airframe icing influence on the unsteady aerodynamics and flight dynamics of the transport aircraft is presented in the current paper. Strong coupling between the flow field dynamics and flight dynamics of the iced aircraft is manifested. In the pre-stall region, evolution of a spanwise-running vortex along the leading-edge separation bubble above the upper surface of the wing was the dominant feature of the flow field. Interaction of this vortex dynamics with manoeuvers of the aircraft plays a crucial role in the flight dynamics in the stall region.

At the first stage of this research, the experimental study of steady and unsteady aerodynamic characteristics was done. The wind tunnel investigation of longitudinal aerodynamic characteristics of the subscale aircraft model was carried out in low-subsonic TsAGI wind tunnel. The aircraft model was the low-wing monoplane with the high aspect ratio wing, the conventional tail unit with the single vertical stabilizer and two wing-mounted engines. Influence produced by the large, glaze-horn icing corresponding to the holding phase was of particular interest.

Through comparison of the wind tunnel results with the flight tests conducted for the real aircraft we proved that the wind tunnel data obtained with small-scale models could be used to predict the behaviour of the aerodynamic characteristics of real aircrafts with large ice shapes quite reasonable.

Negative effects of the airframe icing on the aerodynamics observed in the present study were reduced $C_{L\max}$, decreased C_{L_α}, reduced stall angle, reduced static C_{m_α} and dynamic stability characteristics $C_{m_{\bar{q}}}(\alpha)+C_{m_{\dot{\bar{\alpha}}}}(\alpha)$ in the pre-stall region.

It was found that the stall for the iced wing configurations was observed at the incidence that was two degrees lower, namely, 10 deg instead of 12 deg. The experimental results showed that the wing icing brought the main contribution to degradation of the longitudinal aerodynamic characteristics. The artificial ice shapes on the HT did not influence significantly.

Large, glaze-horn ice shapes corresponding to holding flight phase negatively influenced the longitudinal stability derivatives. Ice shapes caused expansion of the positive damping region into the lower pre-stall AoA region retaining the post-stall AoA without changing, namely, the region became $8 \le \alpha \le 16$ for the iced model instead of $10 \le \alpha \le 16$ for the clean one. In addition, an increase of positive damping peak was also observed for the iced wing configurations.

The heated leading edge IPS installed on the aircraft was shown to cope with the negative effects of the wing icing. In particular, IPS was capable to reduce the lifting force degradation, improving the stability characteristics of the aircraft and decreasing the positive damping peak to the values that were close to the clean wing configurations.

At the second stage of this study, flight dynamics simulation of the iced aircraft was performed. Three different models of aerodynamics were developed and utilized in flight dynamics modelling.

For the first model, the icing effects were taken into account only for the static terms, while for the second model the icing effects were also introduced in the unsteady aerodynamics characteristics. Both models were compared with the non-icing configuration. These three models of aerodynamics were investigated using two-dimensional and four-dimensional longitudinal motion models. Analysis of trim curves revealed that dangerous aircraft behaviour in the form of high-AoA departures and LCO could be observed at smaller elevator deflections for the iced configurations. Taking into account icing influence on the unsteady aerodynamics revealed degradation of the dynamic response and deformation of phase portraits of the system. As a result, even for small AoA and elevator deflections, the aircraft might be trapped into the basin of attraction of high-AoA limit cycle, where a stall of the aircraft can occur.

This study revealed that taking into consideration the icing influence on the unsteady aerodynamic coefficients could prevent from possible underestimation of risk of hazardous phenomena and help to implement more reliable control design.

References

[1] "https://www.faa.gov/documentLibrary/media/Advisory_Circular/AC_25-25A.pdf." .

[2] G. T. Andreev and V. V Bogatyrev, "Investigation Of Icing Effects On Aerodynamic Characteristics Of Aircraft," *Proceedings of ICAS 2014, 29th Congress of the International Council of the Aeronautical Sciences, St. Petersburg, Russia, 7-12 September 2014*. pp. 1–9, 2014.

[3] M. B. Bragg, G. M. Gregorek, and J. D. Lee, "Airfoil aerodynamics in icing conditions," *J. Aircr.*, vol. 23, no. 1, pp. 76–81, Jan. 1986.

[4] H. M. Gurbacki and M. B. Bragg, "Unsteady aerodynamic measurements on an iced airfoil," *40th AIAA Aerosp. Sci. Meet. Exhib.*, no. c, 2002.

[5] L. Prince Raj, J. W. Lee, and R. S. Myong, “Ice accretion and aerodynamic effects on a multi-element airfoil under SLD icing conditions,” *Aerosp. Sci. Technol.*, vol. 85, pp. 320–333, 2019.

[6] M. Costes and F. Moens, “Advanced numerical prediction of iced airfoil aerodynamics,” *Aerosp. Sci. Technol.*, vol. 91, pp. 186–207, 2019.

[7] T. P. Ratvasky, B. P. Barnhart, and S. Lee, “Current methods for modeling and simulating icing effects on aircraft performance, stability and control,” *AIAA Atmos. Flight Mech. Conf. Exhib.*, no. August, pp. 1–21, 2008.

[8] A. Lampton and J. Valasek, “Prediction of icing effects on the lateral/directional stability and control of light airplanes,” *Aerosp. Sci. Technol.*, vol. 23, no. 1, pp. 305–311, 2012.

[9] A. P. Broeren, S. Lee, G. H. Shah, and P. C. Murphy, “Aerodynamic effects of simulated ice accretion on a generic transport model,” *SAE Tech. Pap.*, 2011.

[10] D. Pokhariyal, M. B. Bragg, T. Hutchison, and J. Merret, “Aircraft Flight Dynamics with Simulated Ice Accretion,” in *39th AIAA Aerospace Sciences Meeting & Exhibit 8-11 January 2001*, 2001, no. January.

[11] R. Miller and W. Ribbens, “The Effects of Icing on the Longitudinal Dynamics of an Icing Research Aircraft The University of Michigan AIAA Aerospace Sciences Meeting and Exhibit AIRCRAFT,” *37th AIAA Aerospace Sciences and Meeting & Exhibit*. 1999.

[12] C. Deiler, “Aerodynamic Modeling, System Identification, and Analysis of Iced Aircraft Configurations,” *J. Aircr.*, vol. 55, no. 1, pp. 145–161, Jul. 2017.

[13] M. G. Potapczuk and A. P. Broeren, “An Integrated Approach to Swept Wing Icing Simulation,” *Eur. Conf. Aeronaut. Sp. Sci.*, pp. 1–28, 2017.

[14] Y. Cao, W. Tan, and Z. Wu, “Aircraft icing: An ongoing threat to aviation safety,” *Aerosp. Sci. Technol.*, vol. 75, pp. 353–385, 2018.

[15] N. B. Abramov, M. G. Goman, A. N. Khrabrov, and B. I. Soemarwoto, “Aerodynamic Modeling for Poststall Flight Simulation of a Transport Airplane,” *J. Aircr.*, vol. 56, no. 4, pp. 1427–1440, 2019.

[16] D. I. Ignatyev and A. N. Khrabrov, “Neural network modeling of unsteady aerodynamic characteristics at high angles of attack,” *Aerosp. Sci. Technol.*, vol. 41, 2015.

[17] D. Ignatyev and A. Khrabrov, “Experimental study and neural network modeling of aerodynamic characteristics of canard aircraft at high angles of attack,” *Aerospace*, vol. 5, no. 1, 2018.

[18] B. Pei, H. Xu, and Y. Xue, “Lyapunov Based Estimation of Flight Stability Boundary under Icing Conditions,” *Math. Probl. Eng.*, vol. 2017, 2017.

[19] S. Lee, B. Barnhart, T. P. Ratvasky, E. Dickes, and M. Thacker, “Dynamic wind-tunnel testing of a sub-scale iced business jet,” *Collect. Tech. Pap. - 44th AIAA Aerosp. Sci. Meet.*, vol. 5, no. May 2006, pp. 3186–3199, 2006.

[20] C. Belcastro, “Validation of Safety-Critical Systems for Aircraft Loss-of-Control Prevention and Recovery,” in *AIAA Guidance, Navigation, and Control Conference*, American Institute of Aeronautics and Astronautics, 2012.

[21] D. I. Ignatyev, A. N. Khrabrov, K. A. Kolinko, S. G. Bazhenov, and V. I. Shevyakov, “Experimental Study of Unsteady Aerodynamic Characteristics of Transport Aircraft in Icing Conditions,” *Eucass*, p. 153, 2017.

[22] В. И. Шевяков, “Инженерный метод определения соответствия воздушных судов сертификационным требованиям для условий обледенения,” *Научный вестник Московского государственного технического университета гражданской авиации*, no. 2 (188), pp. 46–52, 2013.

[23] D. I. Poll, “Spiral Vortex Flow Over a Swept-Back Wing.,” *Aeronaut. J.*, vol. 90, no. 895, pp. 185–199, 1986.

[24] M. Goman and A. Khrabrov, “State-space representation of aerodynamic characteristics of an aircraft at high angles of attack,” *J. Aircr.*, vol. 31, no. 5, pp. 1109–1115, 2008.

[25] M. Ghoreyshi, A. Jirásek, and R. M. Cummings, “Computational approximation of nonlinear unsteady aerodynamics using an aerodynamic model hierarchy,” *Aerosp. Sci. Technol.*, vol. 28, no. 1, pp. 133–144, 2013.

[26] M. Tatar and M. Masdari, “Investigation of pitch damping derivatives for the Standard Dynamic Model at high angles of attack using neural network,” *Aerosp. Sci. Technol.*, vol. 92, pp. 685–695, 2019.

[27] M. P. C. van Rooij, N. T. Frink, B. R. Hiller, M. Ghoreyshi, and M. Voskuijl, “Generation of a reduced-order model of an Unmanned Combat Air Vehicle using indicial response functions,” *Aerosp. Sci. Technol.*, vol. 95, p. 105510, 2019.

[28] Y. Yu, H. Yao, and Y. Liu, “Aircraft dynamics simulation using a novel physics-based learning method,” *Aerosp. Sci. Technol.*, vol. 87, pp. 254–264, 2019.

[29] A. Kumar and A. K. Ghosh, “GPR-based novel approach for non-linear aerodynamic modelling from flight data,” *Aeronaut. J.*, vol. 123, no. 1259, pp. 79–92, 2019.

[30] D. I. Ignatyev and A. N. Khrabrov, “Model of the unsteady aerodynamic characteristics at high AOA with nonlinear dependency in angular rate,” in *29th Congress of the International Council of the Aeronautical Sciences, ICAS 2014*, 2014.

[31] M. B. Bragg *et al.*, “Smart icing systems for aircraft icing safety,” *40th AIAA Aerosp. Sci. Meet. Exhib.*, no. January, 2002.

[32] M. G. Goman, G. I. Zagainov, and A. V. Khramtsovsky, “Application of bifurcation methods to nonlinear flight dynamics problems,” *Progress in Aerospace Sciences*, vol. 33, no. 9–10. pp. 539–586, 1997.

[33] Shankar Sastry, *Nonlinear Systems Analysis, Stability, and Control*. Springer-Verlag New York, 1999.

Interplay of unsteady aerodynamics and flight dynamics of transport aircraft in icing conditions

Ignatyev, Dmitry I.

2020-06-11

Ignatyev DI, Khrabrov AN, Kortukova AI, et al., (2020) Interplay of unsteady aerodynamics and flight dynamics of transport aircraft in icing conditions. Aerospace Science and Technology, Volume 104, September 2020, Article number 105914

https://doi.org/10.1016/j.ast.2020.105914